Orientation Relationship between β-Mn and $L2_1$ Matrix in a Cu_2MnAl Alloy

K.C. CHU and T.F. LIU

In the as-quenched condition, the microstructure of the Cu_2MnAl alloy was $L2_1$ phase containing extremely fine L-J precipitates. This result is different from that reported by other workers in the as-quenched Cu_2MnAl alloy. When the as-quenched alloy was aged at 350 °C, γ-brass precipitates started to appear within the $L2_1$ matrix. The orientation relationship between the γ-brass and the $L2_1$ matrix was determined to be cubic to cubic. This result is consistent with that observed by other workers in the aged Cu-Mn-Al alloy. When the alloy was aged at 460 °C, the γ-brass precipitates disappeared and platelike β-Mn precipitates occurred within the $L2_1$ matrix. As the aging temperature was increased to 560 °C, the morphology of the β-Mn precipitates changed from platelike to granular shape. Electron diffraction examinations indicated that in spite of the morphology change the same orientation relationship between the β-Mn and the $L2_1$ matrix is maintained, and it could be best stated as follows:

$$(210)_{\beta\text{-Mn}}//(100)_m,\ (\bar{1}20)_{\beta\text{-Mn}}//(010)_m,\ (001)_{\beta\text{-Mn}}//(001)_m$$

This result is in disagreement with that reported by Kuzobski *et al.* in the aged Cu_2MnAl alloy. In their study, it was concluded that both the morphology of the β-Mn precipitates and the orientation relationship between the β-Mn and the $L2_1$ matrix would vary with the aging temperature.

I. INTRODUCTION

THE as-quenched microstructures of the $Cu_{3-x}Mn_xAl$ ($0.5 \leqq x \leqq 1$) alloys have been studied by many workers.[1–18] In their studies, it is seen that when the $Cu_{3-x}Mn_xAl$ alloys with $0.5 \leqq x \leqq 0.8$ were solution heat treated at a point in the single β phase (disordered body-centered cubic) region and then quenched into iced brined rapidly, a $\beta \rightarrow B2 \rightarrow D0_3 + L2_1$ phase transition occurred during quenching;[1] as the manganese content in the $Cu_{3-x}Mn_xAl$ alloy was increased to 25 at. pct ($x = 1$), the as-quenched microstructure of the Cu_2MnAl alloy became a single $L2_1$ phase.[2–7] In 1995, the present workers performed transmission electron microscopy observations on the phase transformations of a $Cu_{2.2}Mn_{0.8}Al$ alloy.[8] Consequently, we found that a new type of precipitate (designated as L-J phase) with two variants could be observed within the ($D0_3 + L2_1$) matrix in the as-quenched $Cu_{2.2}Mn_{0.8}Al$ alloy. The L-J phase has an orthorhombic structure with lattice parameters $a = 0.413$ nm, $b = 0.254$ nm, and $c = 0.728$ nm. The orientation relationship between the L-J phase and the matrix was $(100)_{L\text{-}J}//(0\bar{1}1)_m$, $(010)_{L\text{-}J}//(1\bar{1}\bar{1})_m$, and $(001)_{L\text{-}J}//(211)_m$. The rotation axis and rotation angle between two variants of the L-J phase were [021] and 90 deg. It is worthwhile to note here that the L-J phase had never been found previously by other workers in the Cu-Al, Cu-Mn, and Cu-Mn-Al alloy systems.

When the $Cu_{3-x}Mn_xAl$ alloys were aged at temperatures ranging from 350 °C to 450 °C, γ-brass precipitates were formed within the matrix.[9–15] The γ-brass precipitate has a $D8_3$ (ordered body-centered cubic) structure with lattice parameter $a = 0.872$ nm.[9,10] The orientation relationship between the γ-brass and the matrix was cubic to cubic.[14,15] When the aging temperature was kept in the range from 460 °C to 650 °C, β-Mn precipitates started to appear within the matrix.[9,15–17] The β-Mn precipitate has an A13 (simple cubic) structure with lattice parameter $a = 0.641$ nm.[9] Although the β-Mn precipitate has been extensively reported to be detected in the aged Cu-Mn-Al alloys, we are aware of only one article concerning the orientation relationship between the β-Mn and matrix.[13] In 1987, Kozubski *et al.* reported that both the morphology of the β-Mn precipitates and the orientation relationship between the β-Mn and the $L2_1$ matrix would vary with the aging temperature; at 460 °C, the morphology of the β-Mn was irregular shape with $[011]_{\beta\text{-Mn}}//[013]_m$, $(100)_{\beta\text{-Mn}}//(100)_m$; at 560 °C, the morphology of the β-Mn was lamellar shape with $[001]_{\beta\text{-Mn}}//[001]_m$, $(210)_{\beta\text{-Mn}}//(100)_m$. Recently, we have also made transmission electron microscopy observations on the phase transformations of the Cu_2MnAl alloy. Based on our present study, it is found that the precipitation behavior of the γ-brass was consistent with that reported by other workers. However, the experimental result concerning the orientation relationship between the β-Mn and the $L2_1$ matrix was different from that reported by Kozubski *et al.*

II. EXPERIMENTAL PROCEDURE

The Cu_2MnAl alloy was prepared in a vacuum induction furnace under a controlled protective argon atmosphere by using 99.99 pct copper, 99.9 pct manganese, and 99.99 pct aluminum. The melt was chill cast into a 30 × 50 × 200-mm copper mold. After being homogenized at 850 °C for 72 hours, the ingot was sectioned into 2-mm-thick slices. These slices were subsequently solution heat treated at 850 °C for 1 hour and then rapidly quenched into iced brine. The aging processes were performed at temperatures ranging

K.C. CHU, Graduate Student, and T.F. LIU, Professor and Chairman, are with the Department of Materials Science and Engineering, National Chiao Tung University, Taiwan 30049, Republic of China.

Manuscript submitted January 30, 1998.

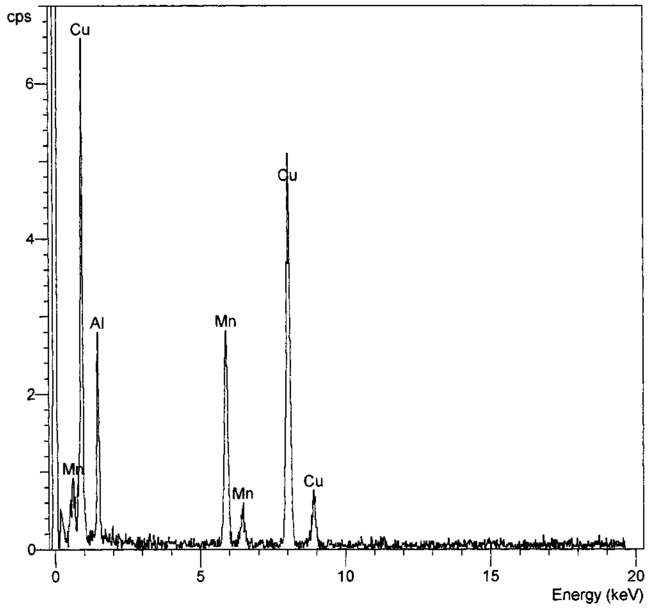

Fig. 1—A typical EDS profile of the present alloy in the as-quenched condition.

from 350 °C to 560 °C for various times in a salt bath and then rapidly quenched into iced brine.

Electron microscopy specimens were prepared by means of a double-jet electropolisher with an electrolyte of 70 pct methanol and 30 pct nitric acid. The polishing temperature was kept in the range from −40 °C to −30 °C, and the current density was kept in the range from 3.0×10^4 to 4.0×10^4 A/m^2. Electron microscopy was performed on a JEOL* 2000FX scanning transmission electron microscope (STEM) operating at 200 kV. This microscope was equipped with a Link ISIS 300 energy-dispersive X-ray spectrometer (EDS) for chemical analysis. Quantitative analyses of elemental concentrations for Cu, Mn, and Al were made with the aid of a Cliff–Lorimer Ratio Thin Section method.

*JEOL is a trademark of Japan Electron Optics Ltd., Tokyo.

III. RESULTS AND DISCUSSION

A typical EDS profile of the alloy in the as-quenched condition is shown in Figure 1. The quantitative analyses of ten different EDS profiles indicated that the average chemical composition was Cu-(25.98 ± 0.04) wt pct Mn-(13.04 ± 0.02) wt pct Al (Cu-(24.68 ± 0.03) at. pct Mn-(25.24 ± 0.02) at. pct Al), which approximates to Cu_2MnAl.

Figure 2(a) is a bright-field (BF) electron micrograph of the as-quenched alloy, exhibiting that a high density of extremely fine precipitates was formed within the matrix. Shown in Figures 2(b) and (c) are two selected-area diffraction patterns (SADPs) of the as-quenched alloy. In the SADPs, it is seen that in addition to the reflection spots corresponding to the $L2_1$ phase,[1,19] the diffraction patterns also consist of extra spots caused by the presence of the extremely fine precipitates. Compared to our previous study in the $Cu_{2.2}Mn_{0.8}Al$ alloy,[8] it is found that these extra spots are of the L-J phase. Figure 2 (d), a (111) $L2_1$ dark-field (DF) electron micrograph, clearly shows the $L2_1$ domains. Figure 2(e) is a DF electron micrograph taken with the reflection spot marked as 1 in Figure 2(b), revealing the presence of the extremely fine L-J precipitates. On the basis of the preceding observations, it is concluded that the microstructure of the alloy in the as-quenched condition is $L2_1$ phase containing extremely fine L-J precipitates.

When the as-quenched alloy was aged at 350 °C, some coarse precipitates with a cuboid shape started to appear within the $L2_1$ matrix. A typical example is shown in Figure 3(a). Figures 3(b) and (c) demonstrate two SADPs taken from an area including the precipitate marked as "R" in Figure 3(a) and its surrounding $L2_1$ matrix. Based on the analyses of the diffraction patterns, it is confirmed that the precipitate has an ordered body-centered cubic structure with lattice parameter $a = 0.872$ nm, which is consistent with that of the γ-brass.[9,10] The orientation relationship between the γ-brass and the $L2_1$ matrix was determined to be $[100]_\gamma // [100]_m$, $(011)_\gamma // (022)_m$. This result is consistent with that reported by other workers in the aged Cu_2MnAl alloy.[12,13]

Transmission electron microscopy examinations of thin foils indicated that the γ-brass precipitates could exist up to 450 °C. However, when the alloy was aged at 460 °C, the γ-brass precipitates disappeared and platelike precipitates occurred within the $L2_1$ matrix, as illustrated in Figure 4(a). Figure 4(a) is a BF electron micrograph of the alloy aged at 460 °C for 20 hours. Figures 4(b) and (c) show two SADPs taken from the platelike precipitate marked as "B" in Figure 4(a). According to the camera length and the measurement of angles as well as d spacings of the diffraction spots, the crystal structure of the precipitate was determined to be simple cubic with lattice parameter $a = 0.641$ nm, which corresponds to that of the β-Mn.[9] In Figure 4(a), it is clearly seen that the β-Mn precipitates were formed along certain preferred orientations. In order to clarify the orientation relationship between the β-Mn and the $L2_1$ matrix, three β-Mn precipitates, marked as A, B, and C in Figure 4(a), were used. Figures 5(a) through (g) show seven SADPs taken from the precipitate A and its surrounding $L2_1$ matrix. These SADPs were obtained by tilting the specimen about some specific reflections. In these figures, the zone axes of precipitate A and the $L2_1$ matrix are $[20\bar{1}]_{PA}$ and $[100]_m$, $[100]_{PA}$ and $[201]_m$, $[301]_{PA}$ and $[101]_m$, $[101]_{PA}$ and $[103]_m$, $[311]_{PA}$ and $[212]_m$, $[321]_{PA}$ and $[111]_m$, and $[210]_{PA}$ and $[211]_m$, respectively. The electron diffractions were also performed to include precipitate B and its surrounding $L2_1$ matrix. The results are shown in Figures 6(a) through (d). The zone axes are $[100]_{PB}$ and $[100]_m$, $[213]_{PB}$ and $[111]_m$, $[221]_{PB}$ and $[110]_m$, and $[110]_{PB}$ and $[22\bar{1}]_m$. Similarly, Figures 7(a) through (e) show five SADPs taken from precipitate C and its surrounding $L2_1$ matrix. The zone axes are $[210]_{PC}$ and $[100]_m$, $[211]_{PC}$ and $[201]_m$, $[212]_{PC}$ and $[101]_m$, $[201]_{PC}$ and $[2\bar{1}1]_m$, and $[100]_{PC}$ and $[2\bar{1}0]_m$. The key diagrams of Figures 5 through 7 are shown in Figures 8 through 10, respectively.

Based on the preceding SADPs, three stereographic projections of the plane normals of the β-Mn precipitates relative to a particular projection of the $L2_1$ matrix can be constructed, respectively. In Figure 5(a), it is obvious that the (102) and (010) reflection spots of the β-Mn are nearly parallel to the (002) and (020) reflection spots of the $L2_1$ matrix, respectively. Using this information, a stereographic

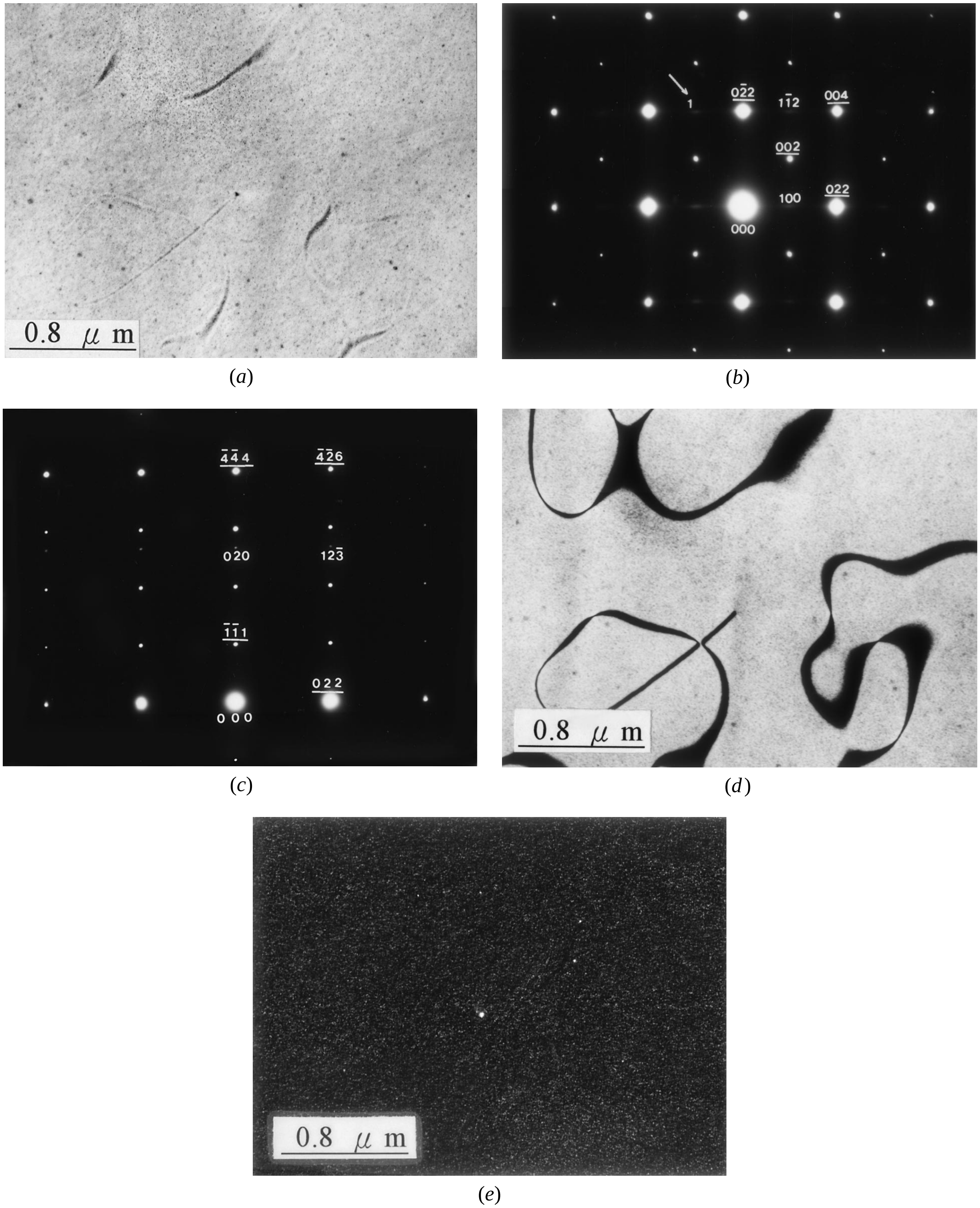

(*a*) (*b*) (*c*) (*d*) (*e*)

Fig. 2—Electron micrographs of the as-quenched alloy: (*a*) BF and (*b*) and (*c*) two SADPs. The zone axes of the $L2_1$ matrix are [100] and [$2\bar{1}1$], respectively (hkl: $L2_1$, hkl: L-J). (*d*) 111 $L2_1$ DF and (*e*) DF, which was taken with the reflection spot marked as 1 in (b).

plot of poles (superimposing the (102) projection of the β-Mn and the (001) projection of the $L2_1$ matrix) was constructed, as shown in Figure 11, where the (010) pole of the β-Mn was made to match with the (010) pole of the $L2_1$ matrix. In this stereographic plot, it is found that the (001), ($\bar{1}03$), ($\bar{1}01$), (112), (122), ($\bar{1}23$), and ($\bar{2}41$) poles of the β-Mn would exactly or nearly coincide with the ($\bar{1}02$), ($\bar{1}01$), ($\bar{3}01$), (012), (011), ($\bar{1}11$), and ($\bar{1}20$) poles of the $L2_1$ matrix. These results are indeed in agreement with those observed in the SADPs shown in Figures 5(a) through (g). Similarly, two stereographic projections concerning the precipitates B and C and the $L2_1$ matrix were also constructed by means of the reflection spots present in Figures 6 and 7. The results are shown in Figures 12 and 13, respectively. Evidently, it

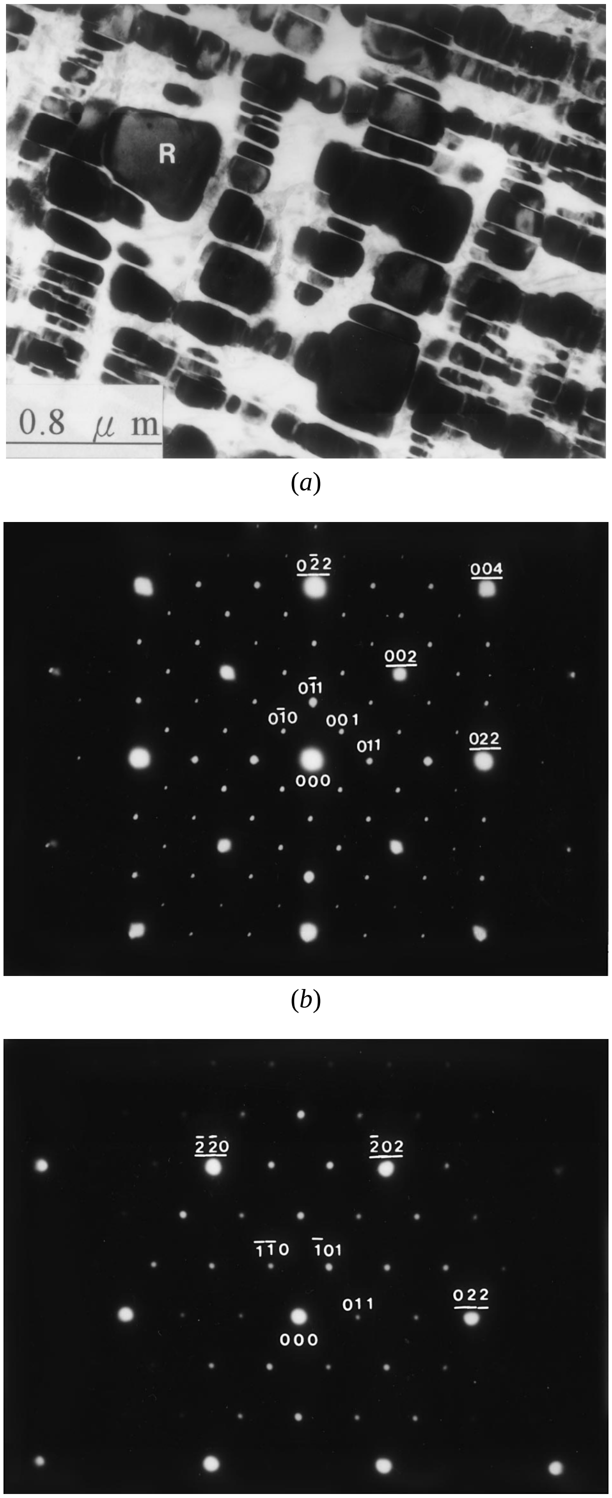

Fig. 3—Electron micrographs of the alloy aged at 350 °C for 30 h. (*a*) BF and (*b*) and (*c*) two SADPs taken from an area including the precipitate marked as "R" in (a) and its surrounding $L2_1$ matrix. The zone axes of the matrix are [100] and [1$\bar{1}$1], respectively (<u>hkl</u>: $L2_1$, hkl: γ-brass).

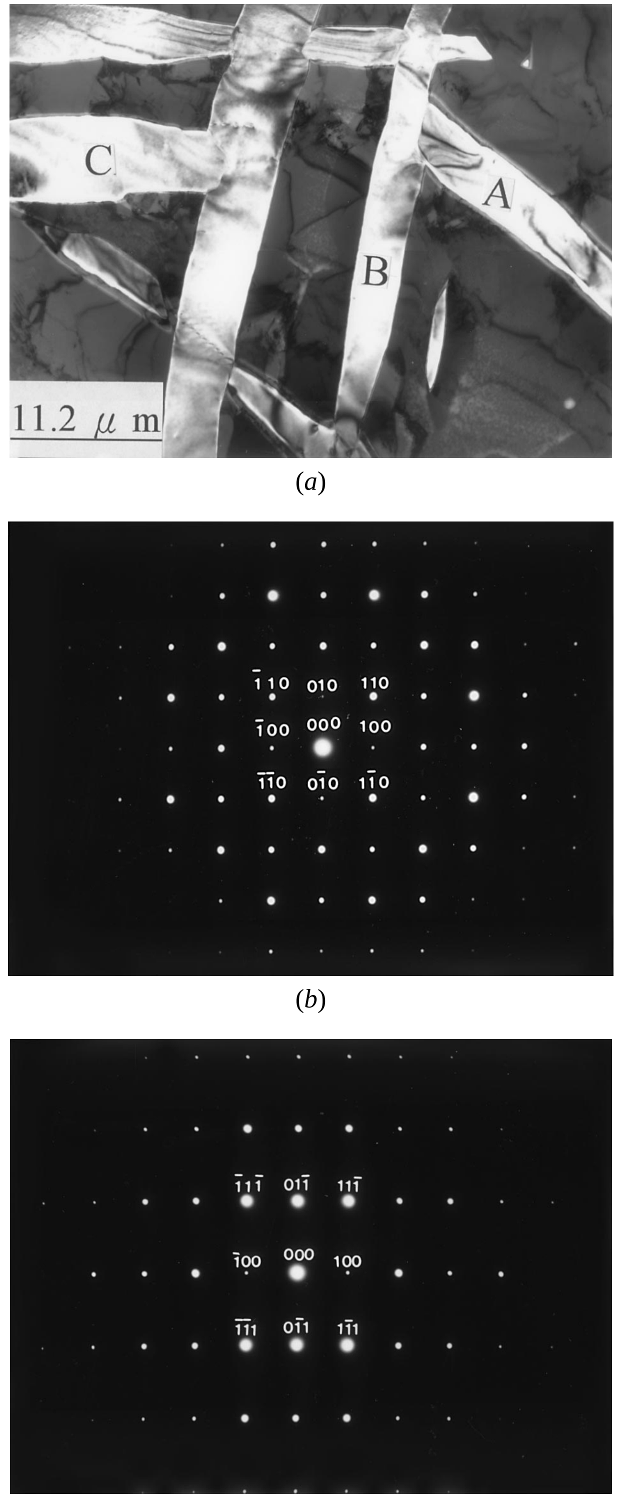

Fig. 4—Electron micrographs of the alloy aged at 460 °C for 20 h. (*a*) BF and (b) and (c) two SADPs taken from the precipitate marked as "B" in (a). The zone axes of the β-Mn are [100] and [101], respectively.

is seen in Figures 11 through 13 that the (102), (010), and ($\bar{2}$01) poles of precipitate A would exactly coincide with the (001), (010), and ($\bar{1}$00) poles of the $L2_1$ matrix; the (0$\bar{1}$2), (021), and ($\bar{1}$00) poles of precipitate B would exactly coincide with the (001), (010), and ($\bar{1}$00) poles of the $L2_1$ matrix; the (001), ($\bar{1}$20), and ($\bar{2}$10) poles of precipitate C would exactly coincide with the (001), (010), and ($\bar{1}$00) poles of the $L2_1$ matrix. This means that when one of the ⟨100⟩ poles of the $L2_1$ matrix coincides with one of the ⟨100⟩

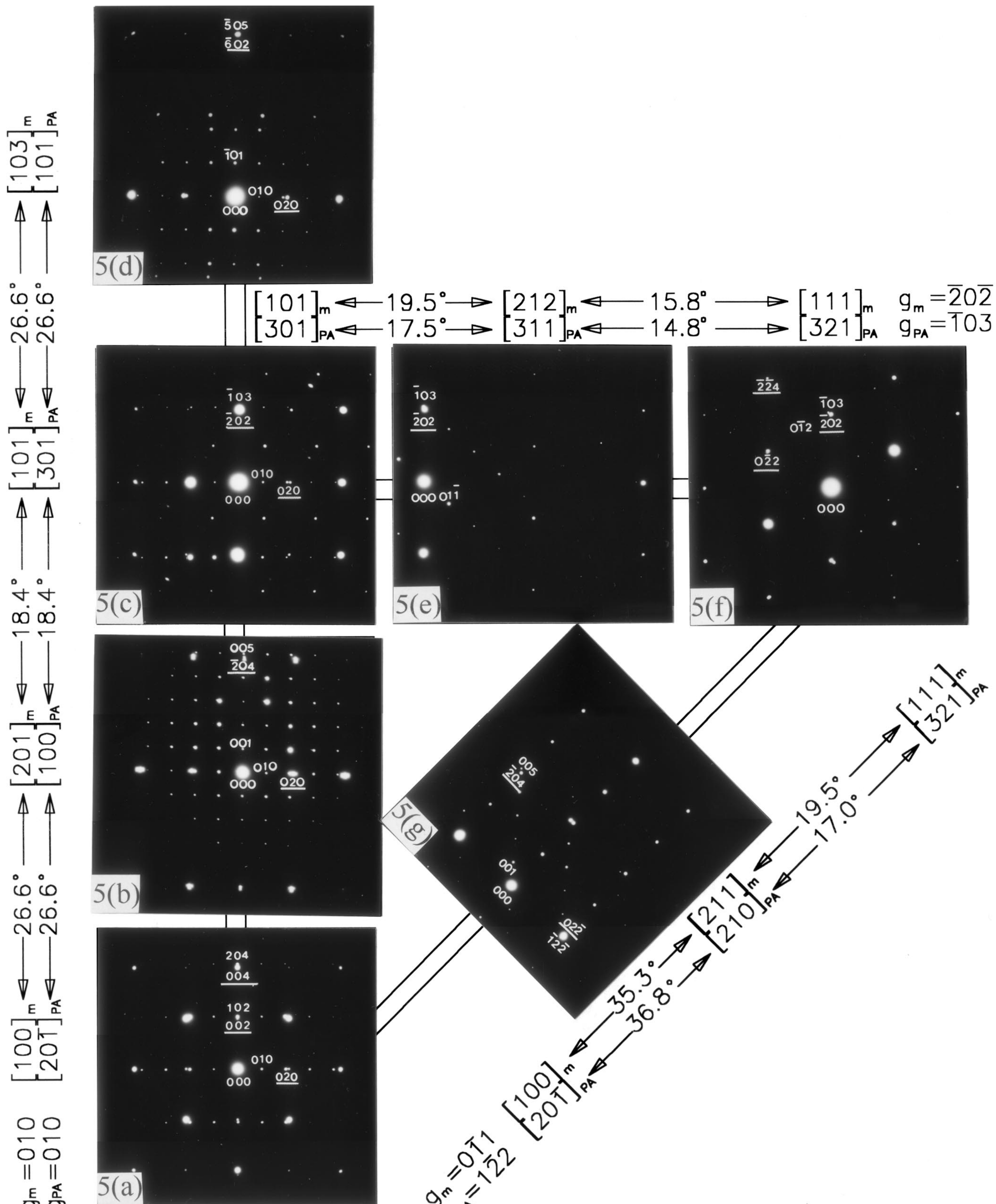

Fig. 5—Seven SADPs taken from an area including the precipitate marked as "A" in Fig. 4(a) and its surrounding $L2_1$ matrix. The zone axes of the $L2_1$ matrix are (*a*) [100], (*b*) [201], (*c*) [101], (*d*) [103], (*e*) [212], (*f*) [111], and (*g*) [211]. (hkl: $L2_1$, hkl: β-Mn).

poles of the β-Mn, the other two ⟨100⟩ poles of the $L2_1$ matrix would coincide with two different ⟨120⟩ poles of the β-Mn. On the basis of the preceding analyses, it is clear that all three precipitates have the same orientation

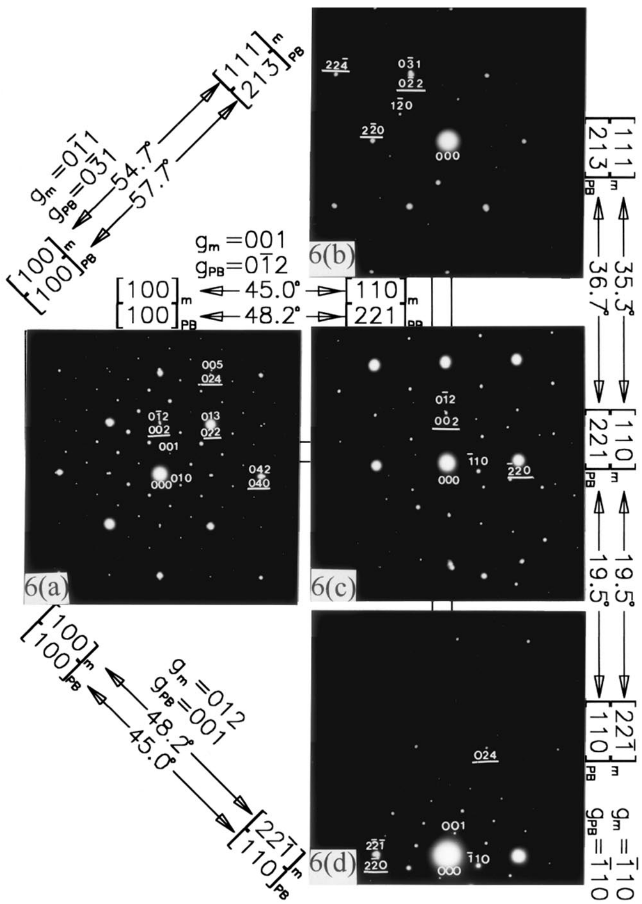

Fig. 6—Four SADPs taken from an area including the precipitate marked as "B" in Fig. 4 (a) and its surrounding $L2_1$ matrix. The zone axes of the $L2_1$ matrix are (*a*) [100], (*b*) [111], (*c*) [110], and (*d*) $[22\bar{1}]$ ($\underline{hkl}$: $L2_1$, hkl: β-Mn).

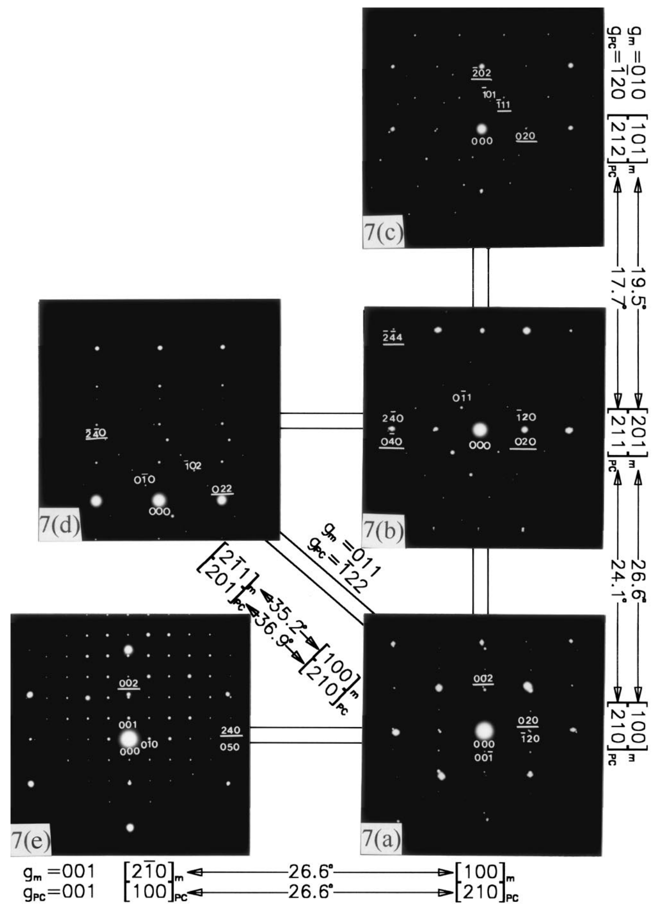

Fig. 7—Five SADPs taken from an area including the precipitate marked as "C" in Fig. 4 (a) and its surrounding $L2_1$ matrix. The zone axes of the $L2_1$ matrix are (*a*) [100], (*b*) [201], (*c*) [101], (*d*) $[2\bar{1}1]$, and (*e*) $[2\bar{1}0]$ ($\underline{hkl}$: $L2_1$, hkl: β-Mn).

relationship with the $L2_1$ matrix, and it can be best stated as follows:

$$(210)_{\beta\text{-Mn}}//(100)_m,\ (\bar{1}20)_{\beta\text{-Mn}}//(010)_m,\ (001)_{\beta\text{-Mn}}//(001)_m$$

In order to further verify the determined orientation relationship between the β-Mn and the $L2_1$ matrix, the Goux method was used.[20] It is seen in Figures 5(a) through (d) that the zone axis of precipitate A is nearly parallel to the corresponding zone axis of the $L2_1$ matrix. Therefore, these four pairs of the parallel zone axes were used to analyze the orientation relationship between precipitate A and the $L2_1$ matrix. In Figure 5(a), the $[20\bar{1}]$ direction of precipitate A is parallel to the [100] direction of the $L2_1$ matrix, so the axis of rotation must be on a zone equiangle from $[20\bar{1}]$ and [100] poles. This is the great circle bisecting the great circle through $[20\bar{1}]$ and [100] poles. The bisecting great circle is marked as "5(a)" in Figure 14, which is a [100] standard stereographic projection. The other bisecting great circles obtained from the analyses of Figures 5(b) through (d) are also drawn in Figure 14, marked as "5(b)", "5(c)", and "5(d)", respectively. It is clearly seen that the four bisecting great circles intersect at the [010] pole. The result indicates that the axis of rotation between precipitate A and the $L2_1$ matrix is [010]. The angle of rotation was determined to be 26.6 deg. The similar analyses of Figure 6(a) and Figures 7(a) and (e) show that the axis/angle pairs of rotation between precipitates B and C and the $L2_1$ matrix are [100]/26.6 and [001]/26.6 deg, respectively. The results indeed further clarify the orientation relationship between the β-Mn and the $L2_1$ matrix. For example, both of the rotation angles from [001] to $[\bar{1}02]$ and $[\bar{1}01]$ to $[\bar{3}01]$ about the [010] axis are 26.6 deg, as indicated in Figure 11.

When the alloy was aged at 560 °C, the morphology of the β-Mn precipitates changed from platelike to granular shape, as illustrated in Figure 15(a). A careful electron diffraction examination indicated that the orientation relationship between the β-Mn and the $L2_1$ matrix was the same as that observed at 460 °C. Figure 15(b) is a (111) $L2_1$ DF electron micrograph, clearly revealing the presence of the $L2_1$ domains.

On the basis of the preceding results, some discussions are appropriate. In the present study, it is obvious that in spite of the morphology change, the orientation relationship between the β-Mn and the $L2_1$ matrix would be maintained. This result is in disagreement with that predicated by Kozubski *et al.*,[13] in which they proposed that when the aging temperature was increased from 460 °C to 560 °C, the orientation relationship between the β-Mn precipitate and the $L2_1$ matrix would change from $[011]_{\beta\text{-Mn}}//[013]_m$, $(100)_{\beta\text{-Mn}}//(100)_m$ to $[001]_{\beta\text{-Mn}}//[001]_m$, $(210)_{\beta\text{-Mn}}//(100)_m$. The apparent

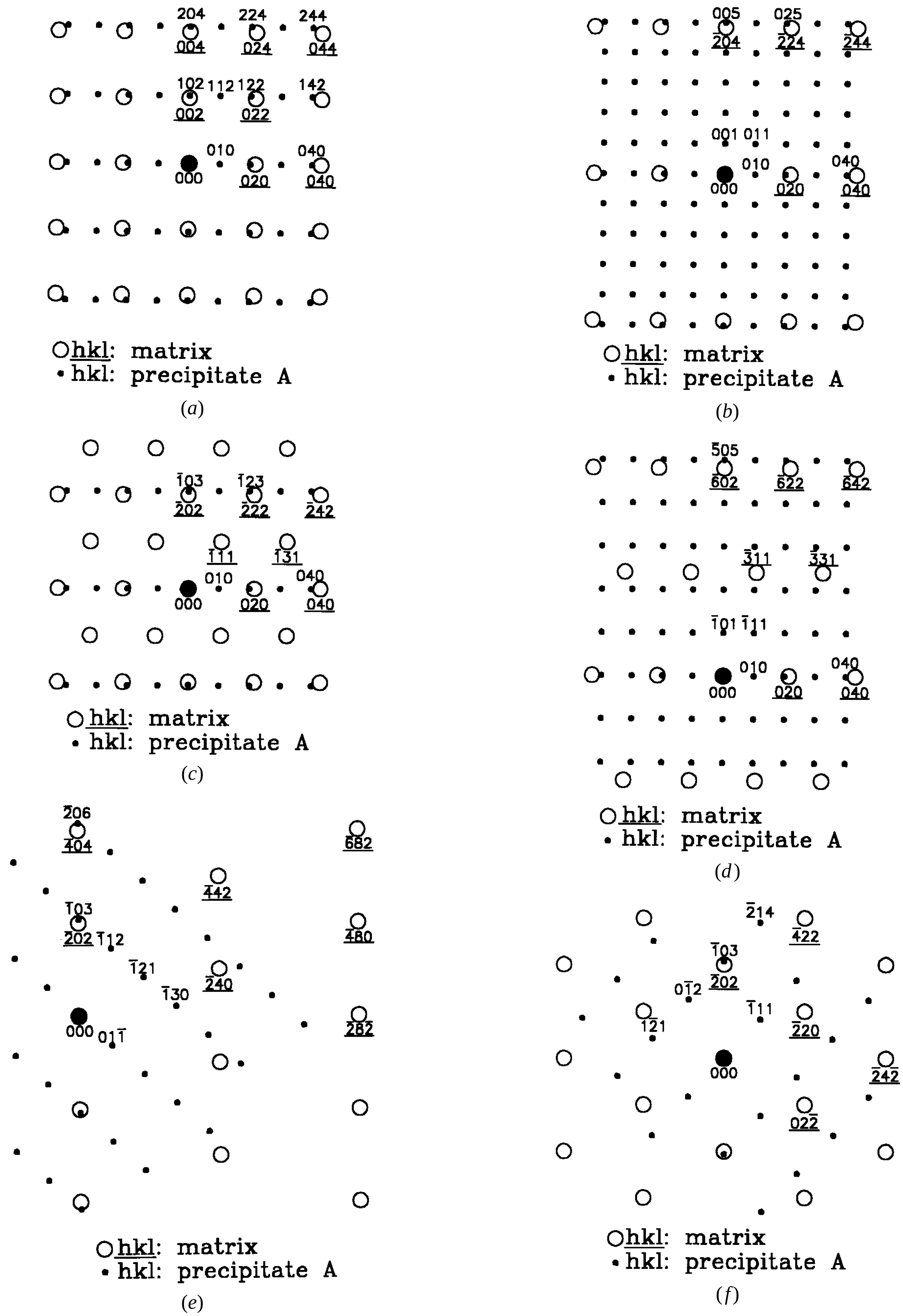

Fig. 8—(*a*) through (*g*) The key diagrams of Figs. 5(a) through (g), respectively. The zone axes are (*a*) $[20\bar{1}]_{PA}$ and $[100]_m$, (*b*) $[100]_{PA}$ and $[201]_m$, (*c*) $[301]_{PA}$ and $[101]_m$, (*d*) $[101]_{PA}$ and $[103]_m$, (*e*) $[311]_{PA}$ and $[212]_m$, (*f*) $[321]_{PA}$ and $[111]_m$.

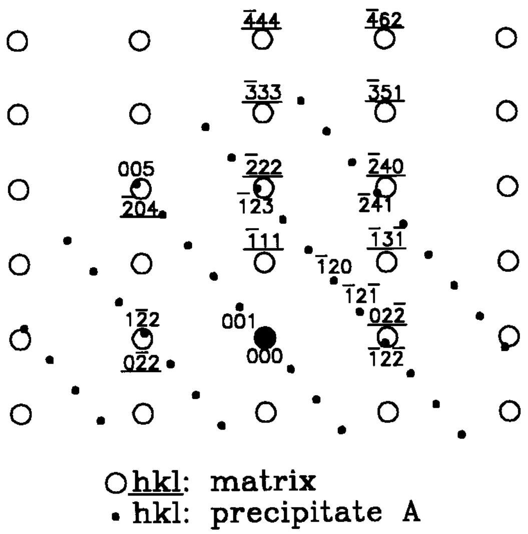

(*g*)

Fig. 8—Continued. (*g*) $[210]_{PA}$ and $[211]_m$ ($\underline{hkl}$: $L2_1$, hkl: precipitate A).

discrepancy can be clarified as follows. In their study, either of the orientation relationships was analyzed by using a single electron diffraction pattern and the two SADPs were taken in $[013]_m$ and $[001]_m$ zone axes, respectively. Accordingly, two different orientation relationships were obtained. In fact, the $[011]_{\beta\text{-Mn}}//[013]_m$, $(100)_{\beta\text{-Mn}}//(100)_m$ and $[001]_{\beta\text{-Mn}}//[001]_m$, $(210)_{\beta\text{-Mn}}//(100)_m$ could be stated as $[\bar{1}01]_{\beta\text{-Mn}}//[\bar{3}01]_m$, $(010)_{\beta\text{-Mn}}//(010)_m$ and $[010]_{\beta\text{-Mn}}//[010]_m$, $(102)_{\beta\text{-Mn}}//(001)_m$ in crystallographic equivalence. In Figure 11, it is clearly seen that the $(\bar{1}01)$, (010), and (102) poles of the β-Mn would exactly coincide with the $(\bar{3}01)$, (010), and (001) poles of the $L2_1$ matrix. This means that these relationships can be drawn in one superimposed β-Mn/$L2_1$ stereogram. Therefore, it is deduced that the two different orientation relationships predicated by Kozubski *et al.* should be considered to be identical.

According to Cu-Mn binary alloy phase diagram,[21] the β-Mn phase was found to exist only when the manganese content was greater than 73 wt pct (75.8 at. pct) and the temperature was in the range from 700 °C to 1050 °C. However, the β-Mn was always observed in the $Cu_{3-x}Mn_xAl$

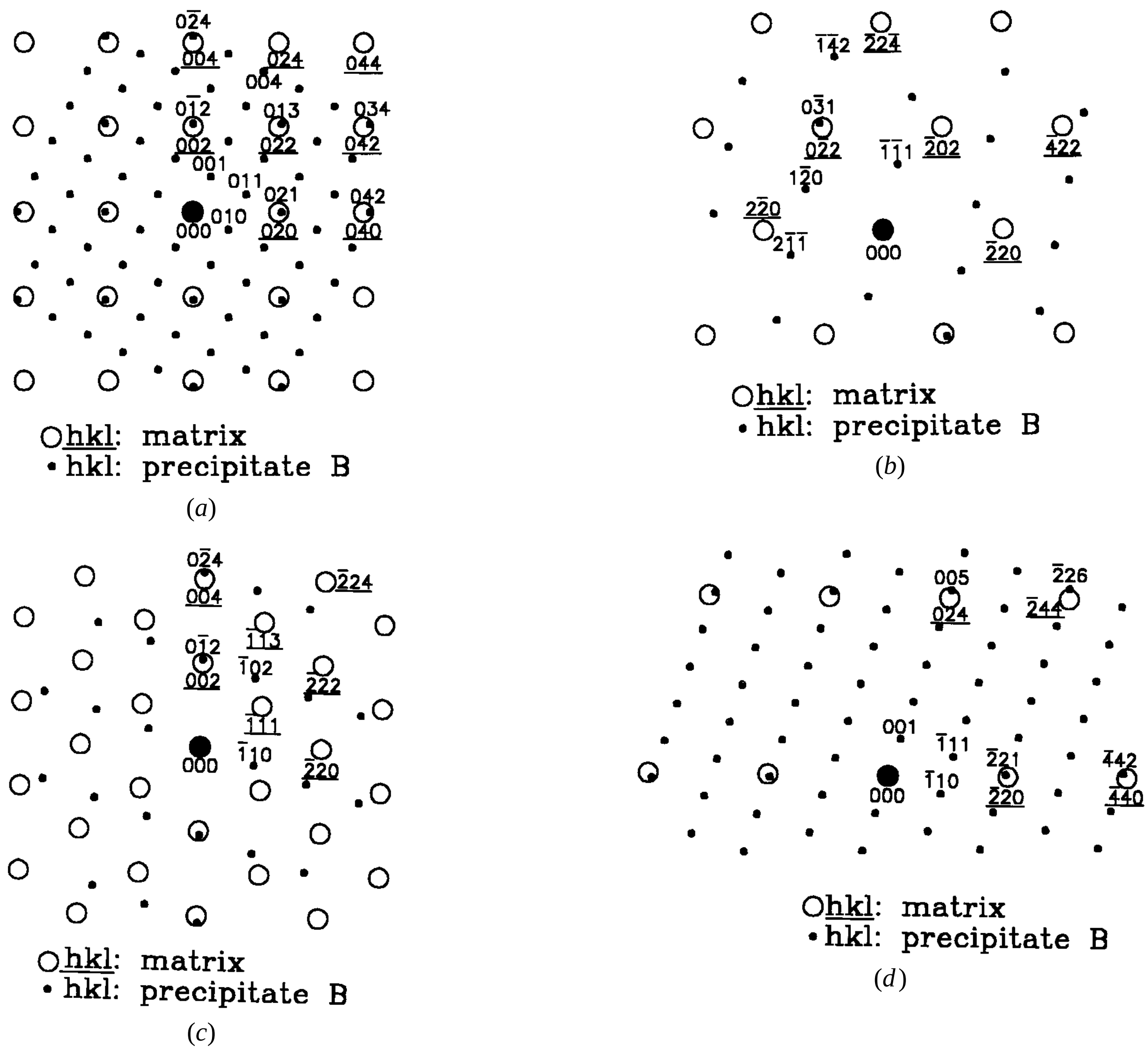

Fig. 9—(*a*) through (*d*) The key diagrams of Figs. 6(a) through (d), respectively. The zone axes are (*a*) $[100]_{PB}$ and $[100]_m$, (*b*) $[213]_{PB}$ and $[111]_m$, (*c*) $[221]_{PB}$ and $[110]_m$, and (*d*) $[110]_{PB}$ and $[22\bar{1}]_m$ ($\underline{hkl}$: $L2_1$, hkl: precipitate B).

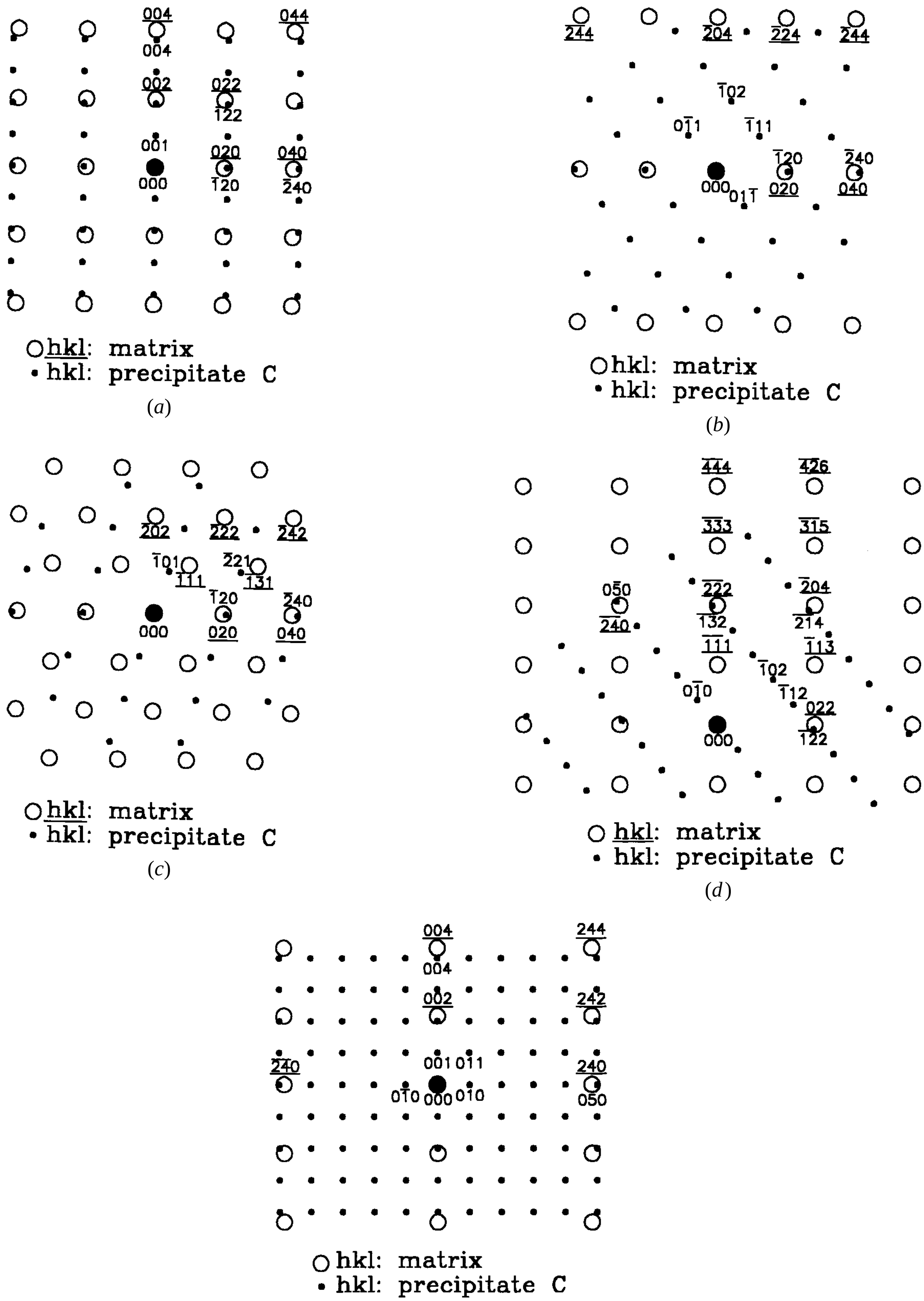

Fig. 10—(*a*) through (*e*) The key diagrams of Figs. 7 (a) through (e), respectively. The zone axes are (*a*) $[210]_{PC}$ and $[100]_m$, (*b*) $[211]_{PC}$ and $[201]_m$, (*c*) $[212]_{PC}$ and $[101]_m$, (*d*) $[201]_{PC}$ and $[2\bar{1}1]_m$, and (*e*) $[100]_{PC}$ and $[2\bar{1}0]_m$, ($\underline{hkl}$: $L2_1$, hkl: precipitate C).

alloys ($0.8 \leqq x \leqq 1$, 20.86 wt pct $\leqq$ Mn $\leqq$ 26.29 wt pct) at 650 °C or below. In order to clarify this feature, an STEM-EDS study was performed. Figure 16 represents a typical EDS profile taken from a β-Mn precipitate in the alloy aged

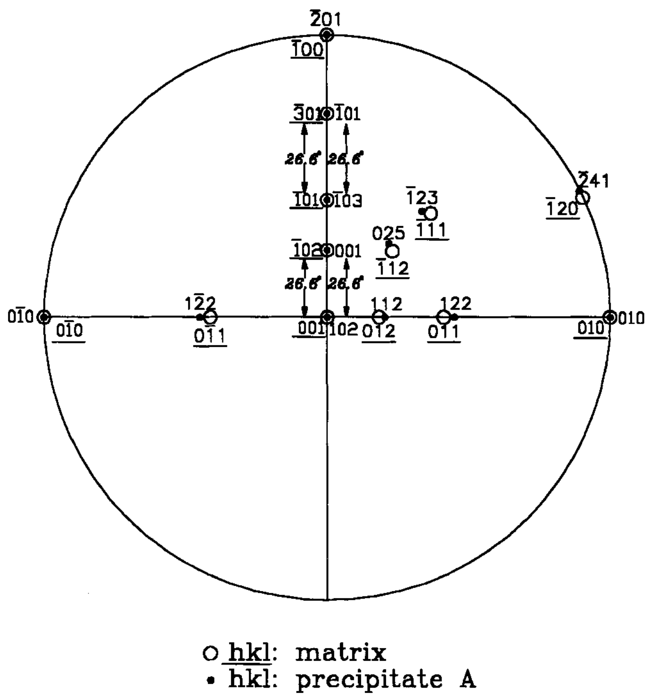

Fig. 11—The superimposed β-Mn/L2_1 stereogram describing the analyses of the SADPs in Figs. 5 (a) through (g).

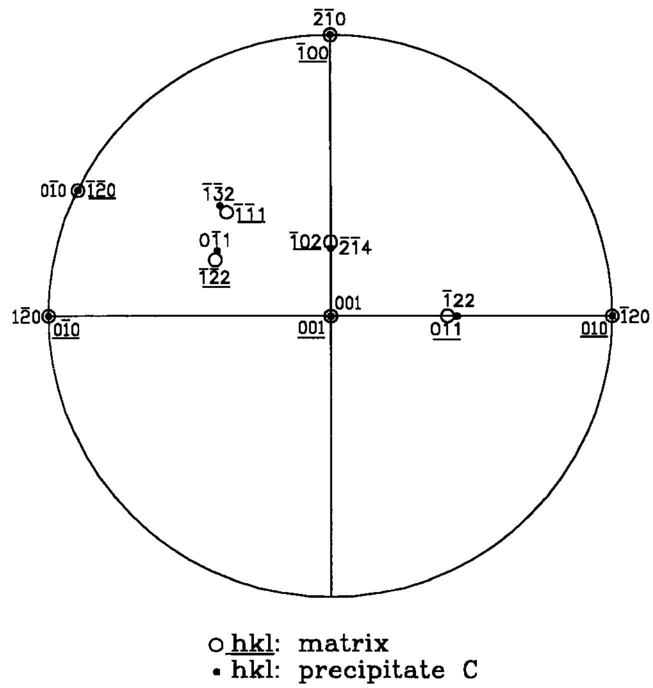

Fig. 13—The superimposed β-Mn/L2_1 stereogram describing the analyses of the SADPs in Figs. 7(a) through (e).

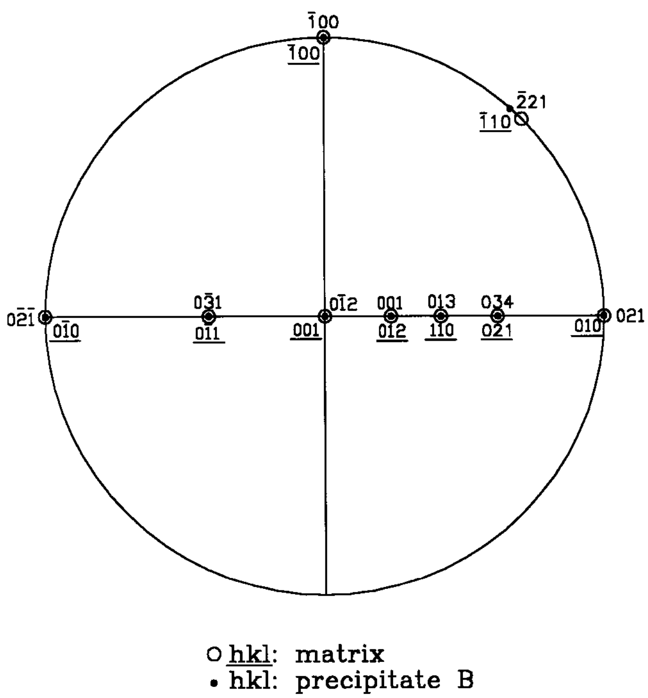

Fig. 12—The superimposed β-Mn/L2_1 stereogram describing the analyses of the SADPs in Figs. 6(a) through (d).

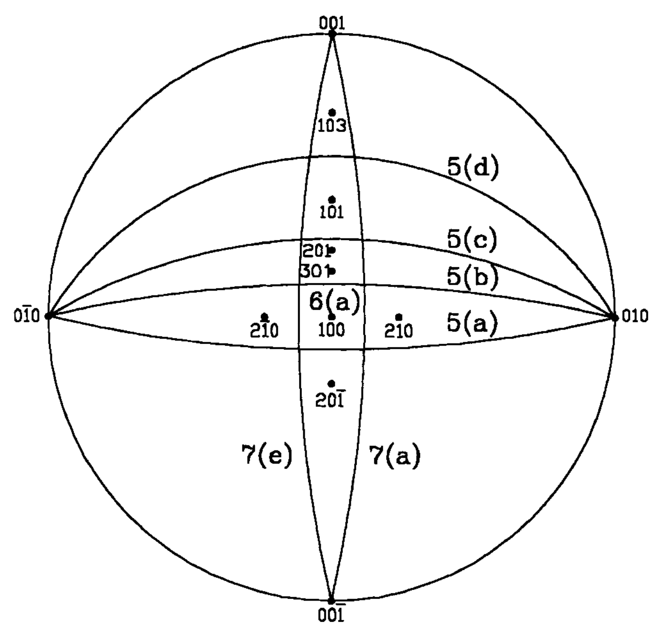

Fig. 14—The stereographic projection describing the Goux analyses of the diffraction patterns of Figs. 5(a) through (d), Fig. 6(a), and Figs. 7(a) and (e).

at 460 °C for 20 hours. The quantitative analyses of ten different EDS profiles revealed that the average weight percentages of the alloying elements in the β-Mn were Cu-(81.03 ± 0.02) pct Mn-(13.99 ± 0.01) pct Al. It is clear that the concentration of copper in the β-Mn was very low. This is similar to that reported by other workers in the Cu-Mn binary alloy, in which they found that the solubility of copper in β-Mn was very small,[21] whereas EDS analyses indicated that the aluminum content in the β-Mn reached to 13.99 wt pct (25.02 at. pct). Thus, it is reasonable to suggest that the aluminum addition in the Cu-Mn binary alloy would pronouncedly expand the β-Mn phase field.

Finally, it is worthwhile to point out that in the present study, the microstructure of the Cu_2MnAl alloy in the as-quenched condition was determined to be L2_1 phase containing extremely fine L-J precipitates. This result is different from that reported by other workers,[1–7] in which they

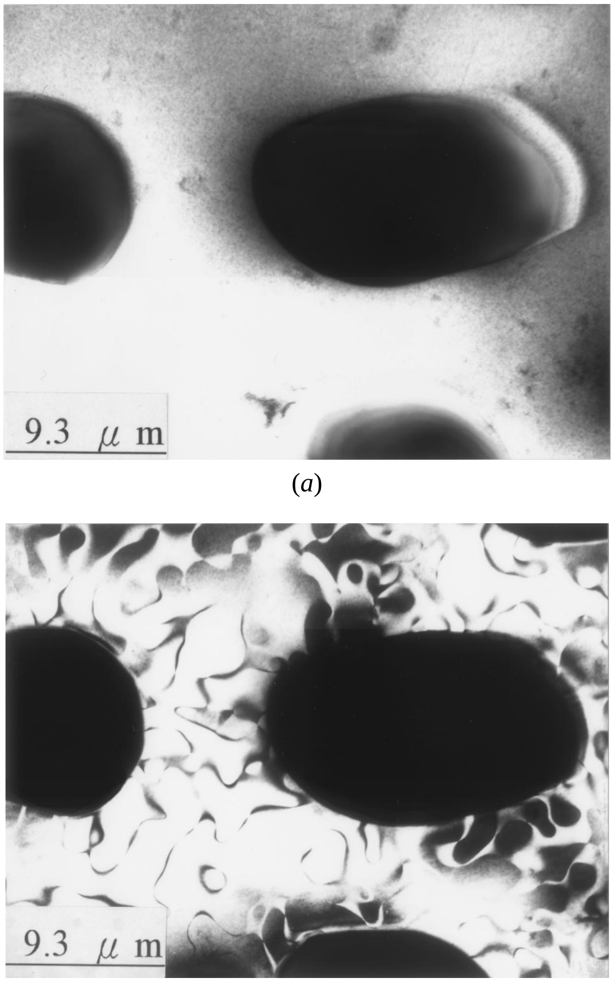

Fig. 15—Electron micrographs of the alloy aged at 560 °C for 10 h: (*a*) BF and (*b*) 111 $L2_1$ DF.

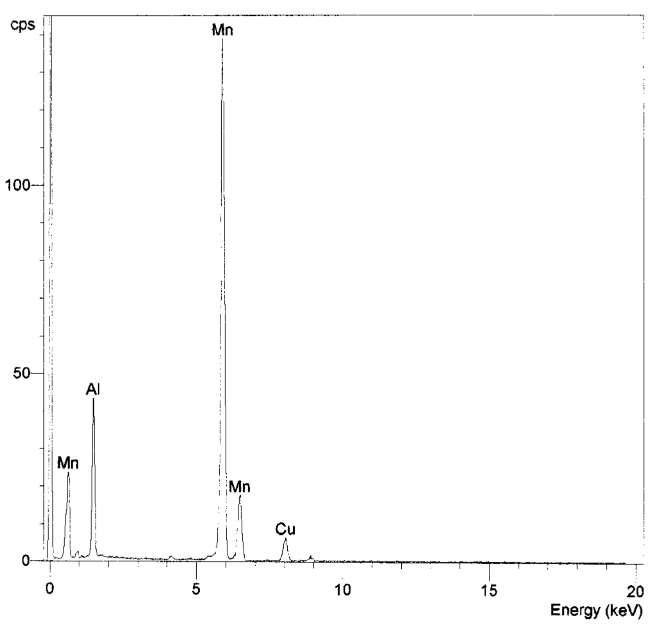

Fig. 16—A typical EDS profile taken from a β-Mn precipitate in the alloy aged at 460 °C for 20 h.

claimed that the as-quenched microstructure of the Cu_2MnAl alloy was a single $L2_1$ phase. The cause of the apparent difference may be attributed to the method of phase identification. In their studies, the microstructure was examined principally by using X-ray diffraction, magnetometry, scanning electron microscopy, and resistometry. These methods may have difficulty detecting the existence of the L-J precipitates, because the amount of L-J precipitates in the as-quenched alloy is very small. It is noted here that in the previous study,[8] we have shown that the amount of the L-J precipitates increased when the $Cu_{2.2}Mn_{0.8}Al$ alloy was aged at 300 °C.

IV. CONCLUSIONS

1. In the as-quenched condition, the microstructure of the Cu_2MnAl alloy was $L2_1$ phase containing extremely fine L-J precipitates.
2. When the alloy was aged at 350 °C, γ-brass precipitates were formed within the $L2_1$ matrix. The orientation relationship between the γ-brass and the $L2_1$ matrix was cubic to cubic.
3. When the alloy was aged at 460 °C, platelike β-Mn precipitates occurred within the $L2_1$ matrix. The orientation relationship between the β-Mn and the $L2_1$ matrix was $(210)_{\beta\text{-Mn}}//(100)_m$, $(\bar{1}20)_{\beta\text{-Mn}}//(010)_m$, $(001)_{\beta\text{-Mn}}//(001)_m$. The rotation axis and rotation angle between the β-Mn and the $L2_1$ matrix were $\langle 100 \rangle$ and 26.6 deg, respectively. When the aging temperature was increased to 560 °C, the morphology of the β-Mn precipitates changed from platelike to granular shape. However, the orientation relationship between the β-Mn and the $L2_1$ matrix was the same as that observed at 460 °C.

ACKNOWLEDGMENTS

The authors are pleased to acknowledge the financial support of this research by the National Science Council, Republic of China, under Grant No. NSC87-2216-E009-008. They are also grateful to Miss M.H. Lin for typing.

REFERENCES

1. M. Bouchard and G. Thomas: *Acta Metall.*, 1975, vol. 23, pp. 1485-1500.
2. Ye.G. Nesterenko, I.A. Osipenko, and S.A. Firstov: *Fiz. Metall. Metalloved.*, 1969, vol. 27, pp. 135-40.
3. Ye.G. Nesterenko, I.A. Osipenko, and S.A. Firstov: *Fiz. Metall. Metalloved.*, 1969, vol. 28, pp. 987-92.
4. Ye.G. Nesterenko, I.A. Osipenko, and S.A. Firstov: *Fiz. Metall. Metalloved.*, 1973, vol. 36, pp. 702-10.
5. V.P. Zalutskiy, Ye.G. Nesterenko, and I.A. Osipenko: *Fiz. Metall. Metalloved.*, 1970, vol. 28, pp. 627-33.
6. Ye.G. Nesterenko and I.A. Osipenko: *Fiz. Metall. Metalloved.*, 1973, vol. 36, pp. 1212-18.
7. G.B. Johnston and E.O. Hall: *J. Phys. Chem. Solids*, 1968, vol. 29, pp. 193-200.
8. S.C. Jeng and T.F. Liu: *Metall. Mater. Trans. A*, 1995, vol. 26A, pp. 1353-66.
9. R. Kozubski and J. Soltys: *J. Mater. Sci.*, 1982, vol. 17, pp. 1441-46.
10. R. Kozubski and J. Soltys: *J. Mater. Sci.*, 1979, vol. 14, pp. 2296-302.
11. R. Kozubski, J. Soltys, and R. Kuziak: *J. Mater. Sci.*, 1983, vol. 18, 3079-86.

12. J. Pons and E. Cesari: *Mater. Sci. Eng.*, 1992, vol. A158, pp. 119-28.
13. R. Kozubski, J. Soltys, J. Dutkiewicz, and J. Morgiel: *J. Mater. Sci.*, 1987, vol. 22, pp. 3843-46.
14. T. Yamane, H. Okamoto, and J. Takahashi: *Z. Metallkd.*, 1980, vol. 71, 813-17.
15. R. Kozubski and J. Soltys: *J. Mater. Sci.*, 1983, vol. 18, pp. 1689-97.
16. R. Kozubski and J. Soltys: *J. Mater. Sci. Lett.*, 1983, vol. 2, pp. 141-43.
17. B. Dubois and D. Chevereau: *J. Mater. Sci.*, 1979, vol 14, p. 2992.
18. J. Soltys, M. Stefaniak, and J. Holender: *Phil. Mag.*, 1984, vol. 49B, pp. 151-58.
19. M.G. Mendiratta, S.K. Ehlers, and H.A. Lipsitt: *Metall. Trans. A*, 1987, vol. 18A, pp. 509-18.
20. J.W. Edington: *The Operation and Calibration of the Electron Microscope*, The MacMillan Press, London, 1975, vol. 1, pp. 42-43.
21. A.H. Sully: *Manganese*, Academic Press, New York, NY, 1955, pp. 189-91.